Flexoelectric barium strontium titanate (BST) hydrophones Ⓕ ⓢⓒⓘ

iD **Michael Hahn,** iD **Susan Trolier-McKinstry, and Richard J. Meyer**

COLLECTIONS

Paper published as part of the special topic on Trends in Flexoelectricity

Ⓕ   This paper was selected as Featured

ⓢⓒⓘ   This paper was selected as Scilight

View Online   Export Citation   CrossMark

ARTICLES YOU MAY BE INTERESTED IN

The impact of flexoelectricity on materials, devices, and physics
Journal of Applied Physics **128**, 080902 (2020); https://doi.org/10.1063/5.0015987

Pressure gradient effect on spin-crossover materials: Experiment vs theory
Journal of Applied Physics **129**, 064501 (2021); https://doi.org/10.1063/5.0042582

Testing flexoelectric device capability as an alternative to piezoelectric technology
Scilight **2021**, 071103 (2021); https://doi.org/10.1063/10.0003542

Flexoelectric barium strontium titanate (BST) hydrophones (SCI) (F)

Michael Hahn,[1,a)] (iD) Susan Trolier-McKinstry,[1] (iD) and Richard J. Meyer, Jr.[2]

AFFILIATIONS

[1]Department of Materials Science and Engineering and Materials Research Institute, Pennsylvania State University, University Park, Pennsylvania 16802, USA
[2]165 Applied Research Laboratory, Pennsylvania State University, University Park, Pennsylvania 16802, USA

Note: This paper is part of the Special Topic on Trends in Flexoelectricity.
[a)]**Author to whom correspondence should be addressed:** mah844psu@gmail.com

ABSTRACT

Flexoelectric hydrophones offer the possibility of reasonable sensitivity in lead-free systems. In this work, a dense barium strontium titanate ceramic with a Ba:Sr ratio of 70:30 and an effective flexoelectric coefficient, $\tilde{\mu}_{12}$, of $105.6 \pm 0.6\,\mu C/m$ at room temperature was utilized in a prototype three-point bending hydrophone with dimensions of $77 \times 10 \times 0.67\ mm^3$. Tap testing of this hydrophone with a calibrated acoustic hammer showed a resonant frequency of 250 Hz and a maximum sensitivity of 80 pC/N. Finite element analysis (FEA) was employed to verify the experimental results and to refine the predictive modeling capability. FEA was used to predict the resonant frequency of devices based on geometry, boundary conditions, and material properties. The error in resonant frequency between the FEA model and the experiment was 7.6%. FEA also enables calculations of the strain gradient produced in a material, allowing the numerical analysis of the element's expected flexoelectric output. Using this technique, single and three bending point hydrophone designs were compared. The results showed a 43% increase in charge output in the three bending point design vs the single bending point design despite an average strain decrease of 48% in each electrode pair. This design would lower the voltage output by 48% in a voltage-based design unless the voltages could be added in series. FEA studies also found the greatest flexoelectric output at low frequencies with improved high frequency output using larger electrode areas.

I. INTRODUCTION

In recent years, flexoelectricity has garnered interest as an alternative to piezoelectricity. Flexoelectricity is a universal phenomenon in all insulating materials. This widened material selection provides alternatives to Pb-based piezoelectric devices, potentially reducing environmental and safety concerns related to Pb. Flexoelectricity may also benefit micro-/nano-electromechanical systems (MEMS) and (NEMS) technologies based on enhanced performance at these scales. Flexoelectricity is driven by strain gradients inside the material; at the micro- and nano-scales, these gradients may be orders of magnitude larger than at bulk scale.[1,2] Besides being Pb-free, flexoelectric materials still have potentially substantial improvements through engineering and design optimization that could increase their sensitivity to on par or greater than current piezoelectric devices such as hydrophones. This may be accomplished by increasing the strain gradient through thinner

elements, multiple bending points, or layering elements together. These factors have driven interest in the phenomenon.

Flexoelectricity is a fourth-rank tensor property that is present in every insulating material. While a uniform strain cannot induce polarization in a centrosymmetric material, a *strain gradient* acts as a vector field, allowing a net polarization to develop. The resulting polarization vector points from the compressive side to the tensile side, assuming a shift in the cation position. For example, it has been reported that in perovskites, the B-site cation induces the flexoelectric polarization.[3]

Flexoelectricity is governed by the following equation:

$$P_l = \mu_{ijkl}\frac{\partial S_{ij}}{\partial x_k},\qquad(1)$$

where P_l is the component of the resultant polarization, μ_{ijkl} are the flexoelectric coefficients (fourth-rank polar tensors), S_{ij} is

the component of elastic strain, and x_k is the direction of the gradient in S.

In 1957, Mashkevich and Tolpygo produced the first theoretical work on the flexoelectric effect.[4] The first phenomenological theory was formulated by Kogan in 1964; Kogan also derived the first order-of-magnitude estimate of the flexocoupling coefficient, f_{ijkl}, which is simply the flexoelectric tensor, μ_{ijkl}, normalized to the dielectric constant of the material, as described in Eq. (2). The flexocoupling coefficient, f, is estimated to be 1–10 V based on the permittivity of free space, ε_o, an atomic charge, q, and an atomic spacing, a, which is on the order of angstroms. The estimate is based on a strain gradient on the order of $1/a$.[5]

$$f \approx \frac{q}{4\pi\varepsilon_o a} \cong 1-10 \text{ V}. \qquad (2)$$

Tagantsev proposed that the flexoelectric coefficient, μ, was directly proportional to the dielectric susceptibility, χ, of the material using the flexocoupling coefficient, f, as described in the following equation:[6–8]

$$\mu = f\chi. \qquad (3)$$

Therefore, the flexoelectric effect is greatest in materials with high permittivity.

II. EXPERIMENTAL PROCEDURE

Barium strontium titanate (BST) cantilever samples from Texas Instruments (TI) were fabricated to measure $\tilde{\mu}_{12}$ using a

method described elsewhere.[9] Electrodes (5 mm wide) were positioned at the clamping end of the beam by sputtering 100 nm of platinum through an aluminum shadow mask using a Quorum EMS 150R S. The electrode radii sizes were approximately 200, 300, 460, and 690 μm. The electrodes were positioned so that the beam was clamped at the edge of the electrodes. The clamped beam dimensions were maintained to approximately a 1:4 width to length ratio, which in this case translated to an $\sim 10 \times 40$ mm^2 BST cantilever sample. Two Omega strain gauges (one for longitudinal and one for lateral strain) were attached to the sample on the clamped edge of the electrodes using cyanoacrylate glue. Sinusoidal strain measurements were made using a quarter Wheatstone bridge configuration attached to a lock-in amplifier (Stanford Research SR830 DSP) at a 30 s time constant. The charge was measured simultaneously with a custom charge integrator circuit optimized for 4 Hz using the same lock-in amplifier at a 30 s time constant. The sample was flexed by a shielded piezoelectric stack actuator (Kinetic Ceramics) with the drive signal generated by the same lock-in amplifier. The setup is pictured in Fig. 1.

The prototype hydrophone was designed based on the work of Chu et al. and is shown in Fig. 2.[10] The aluminum frame and tungsten supports were cut to design dimensions and bonded using epoxy resin, EPON Resin 828, and a curing agent, EPIKURE 3140,

Omega strain gauges (lateral and longitudinal)

40 mm

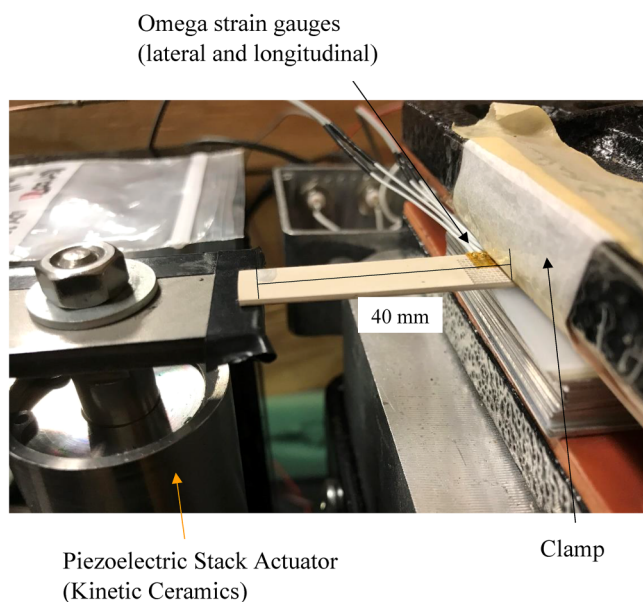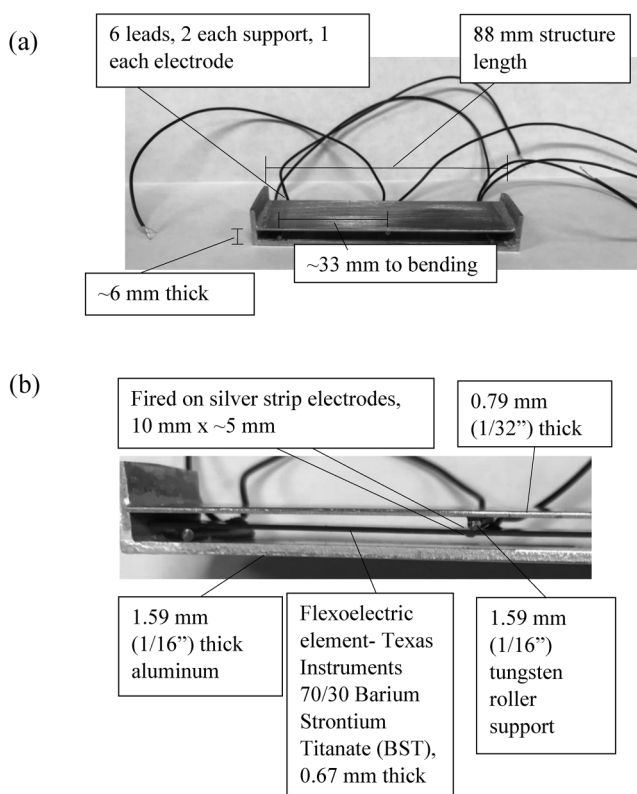Piezoelectric Stack Actuator (Kinetic Ceramics)

Clamp

FIG. 1. Flexoelectric cantilever bending setup with key components labeled. Polarization and strain are measured to calculate the effective flexoelectric coefficient.

(a)

6 leads, 2 each support, 1 each electrode

88 mm structure length

$\sim$6 mm thick

$\sim$33 mm to bending

(b)

Fired on silver strip electrodes, 10 mm x $\sim$5 mm

0.79 mm (1/32") thick

1.59 mm (1/16") thick aluminum

Flexoelectric element- Texas Instruments 70/30 Barium Strontium Titanate (BST), 0.67 mm thick

1.59 mm (1/16") tungsten roller support

FIG. 2. (a) Flexoelectric prototype structure measurements; (b) flexoelectric prototype cross section detailing measurements and materials.

in a 100 to 90 parts mixture. The flexoelectric BST element was bonded to the sidewalls using the same mixture. Fired on silver strip electrodes that were $10 \times \sim 5\,\text{mm}^2$ were centered at the tungsten supports to collect the flexoelectric output.

III. EXPERIMENTAL RESULTS

X-ray diffraction (XRD) measurements of the bulk sample confirmed that the TI BST ceramics were phase pure. The dielectric properties of the TI 70/30 BST given in Fig. 3 were measured using a Delta design 2300 heating/cooling oven. The sample temperature was measured and recorded from a type-K thermocouple using a digital multimeter (Hewlett Packard 3478).

Figure 4 shows the results of the TI BST 70/30 cantilever flexoelectric coefficient measurement. A $\tilde{\mu}_{12}$ was determined to be $105.6 \pm 0.6\,\mu\text{C/m}$, in agreement with previous studies by Ma and Cross.[11]

A tap test was used to assess the functionality of the prototype hydrophone; a calibrated impulse hammer was used to strike the top center of the structure, flexing the element, and thus generating an electrical output. The impulse hammer used was a Model 086C02 from PCB Piezotronics with a stainless steel tip (Model 084B03). Data were collected with a USB-4431 from National Instruments; no pre-amplifier was required. The power spectral density plot vs frequency is given in Fig. 5.

Using the frequency response function (FRF) data shown in Fig. 5 and the sensitivity of the hammer [11.2 mV/N (±15%)], the sensitivity of the hydrophone was measured. The sensitivity in pC/N is displayed in Fig. 6. The maximum coherent sensitivity of 80 pC/N can be compared to bulk PZT d_{33} values of 200–600 pC/N. While below PZT values, this flexoelectric sensitivity includes potential flexoelectric advantages while being Pb-free.
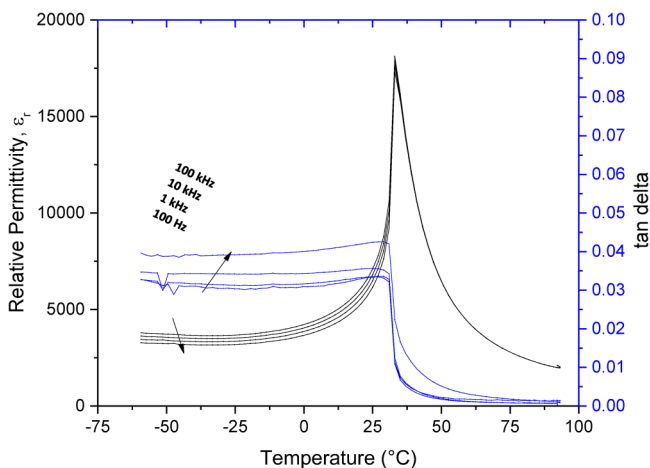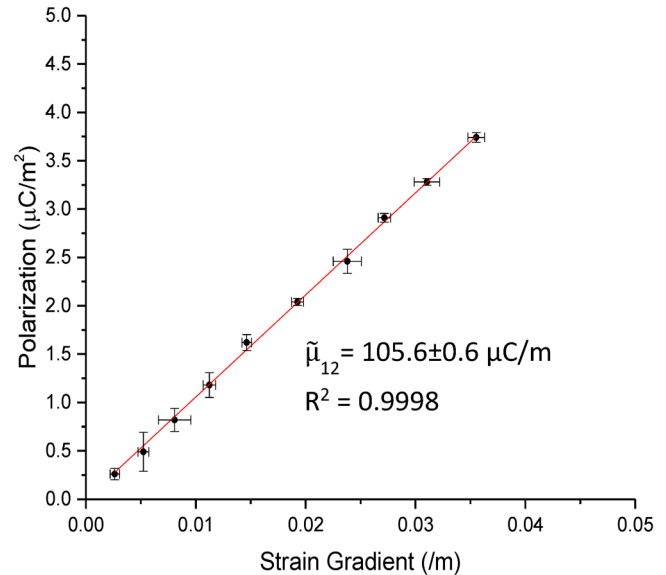

FIG. 4. Cantilever flexoelectric study of BST 70/30 from TI demonstrating a linear flexoelectric behavior and flexoelectric coefficient, $\tilde{\mu}_{12}$, of $105.6 \pm 0.6\,\mu\text{C/m}$.

IV. FINITE ELEMENT ANALYSIS (FEA)

FEA was performed using COMSOL Multiphysics® Modeling Software version 5.4. Cantilever and three-point bending beam geometries were created using the structural mechanics module. Table I provides the constants employed.

A free tetrahedral mesh was used with an element size of 0.5 mm. Figure 7 displays results for the model of the prototype frequency response. A resonant frequency at 268.94 Hz was recorded, giving an error of 7.6% with respect to the experimental value of 250 Hz. This error is reasonable given intrinsic error from error propagation through FEA elements, imperfect boundary conditions, and estimated material properties.

The strain gradient of the material can be visualized and quantified using FEA to allow optimal electrode size and placement. Figure 8 demonstrates a full bending cycle of a BST beam at 4 Hz.

The bending point study shown in Fig. 9 provides insight into design considerations. The average strain of the single electrode and the three-electrode designs were 4.21×10^{-6} and 2.01×10^{-6}, respectively: a 48% decline relative to the one electrode design over a cycle. However, because the three-electrode design harvested electrical output from all three electrode pairs (three times the area) vs the one electrode pair design, the total output of the device was over 43% higher. If the device is a charge-based sensor, larger electrodes and multiple bending points will maximize the charge collected and therefore produce greater output, resulting in better performance. However, if the device is voltage-based, larger electrodes cause parasitic capacitance. The strain gradient is maximized at the center of the electrodes when positioned correctly and declines linearly in both lateral directions resulting in decreased voltage with increased electrode size. This suggests that the optimal
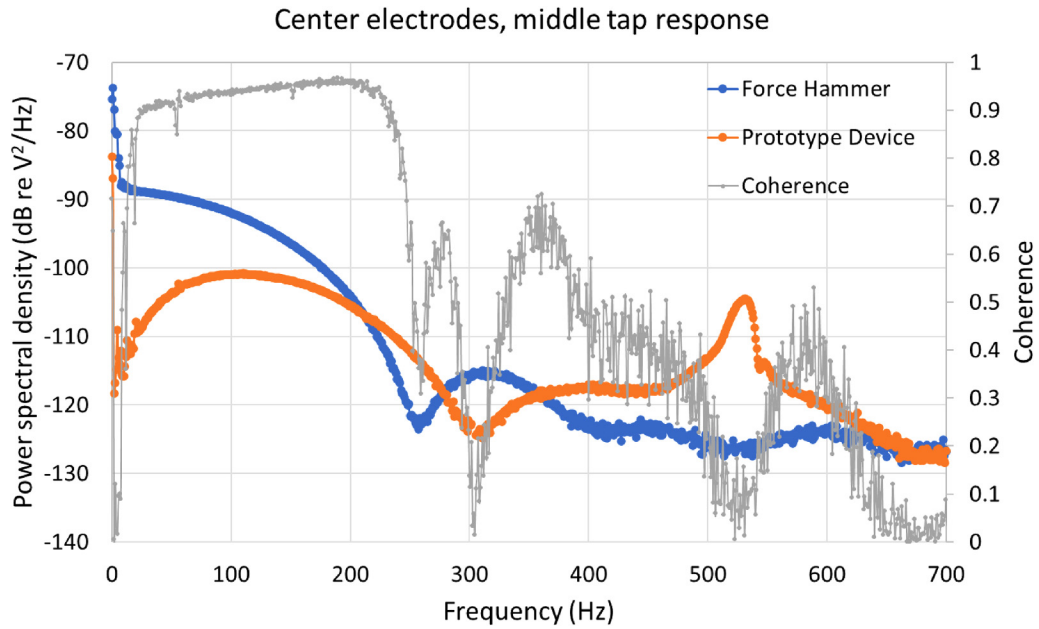

FIG. 3. TI 70/30 BST relative permittivity as a function of temperature from −60 to 93 °C measured on cooling with a maximum permittivity achieved at Curie temperature, 33 °C, of 18 000.

FIG. 5. Flexoelectric prototype frequency response function (FRF) was measured as power spectral density (PSD) vs frequency. The signals are related through coherence values from 0 to 1.
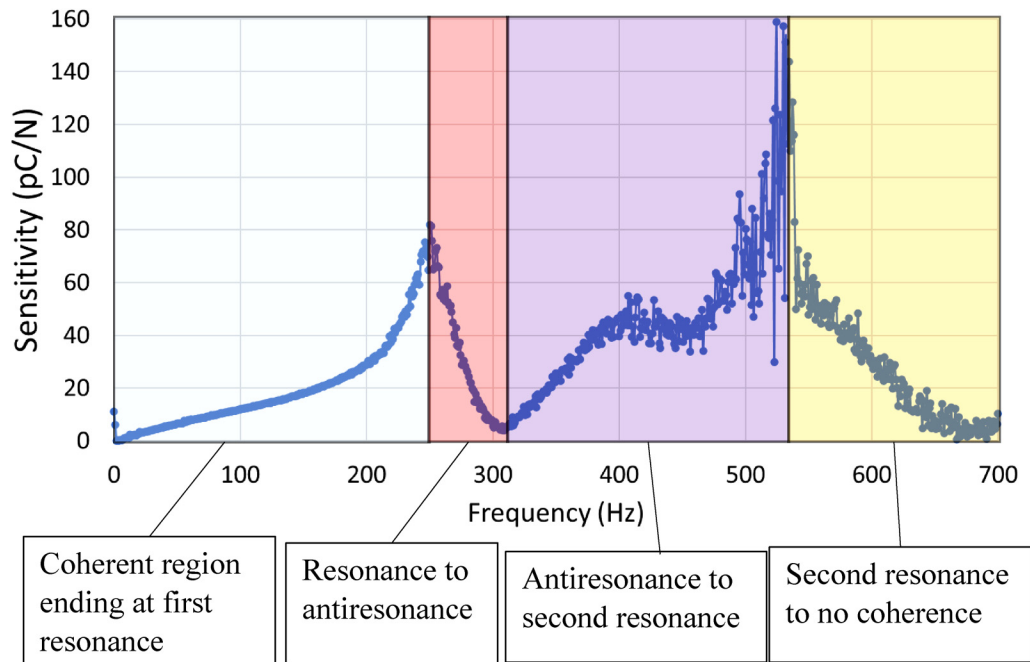

FIG. 6. Flexoelectric prototype sensitivity as a function of frequency calculated from the FRF using the sensitivity of the force hammer and the capacitance of the device. The sensitivity peaks at 80 pC/N at the resonant frequency of 250 Hz and dips to near 0 pC/N at the antiresonant frequency of 300 Hz. Regions of interest are labeled.

TABLE I. FEA BST material constants.

Model parameter	Value
Elastic modulus (GPa)	161
Density (g/cm^3)	5.683
Poisson's ratio	0.35

design for voltage-based devices would utilize the smallest possible electrode area, centered on bending points. Multiple bending points lower the voltage output by decreasing the strain gradient at each electrode pair. Ideally, voltages would be added in series to increase their output. If series connection is not possible, multiple bending points would degrade the voltage output in a voltage-based device.

A similar study investigated the effect of decreasing the thickness of the flexoelectric on the fundamental frequency and average strain gradient of the element. The results are displayed in Fig. 10. The fundamental frequency of the beam decreased linearly with decreasing thickness while the strain gradient increases substantially. For example, by halving the thickness from 0.60 mm to 0.30 mm resulted in around an 8× increase in the strain gradient. The increase in strain gradient is a result of a combination of the reduced flexural rigidity with decreasing thickness and the size effect of decreasing the neutral axis which follows a 1/a (where a is the length scale) mathematical relationship. The expected flexoelectric output is directly correlated to the strain gradient.

Finally, the addition of fixed-fixed bending points on the fundamental frequency and strain gradient was investigated. The results are provided in Fig. 11.
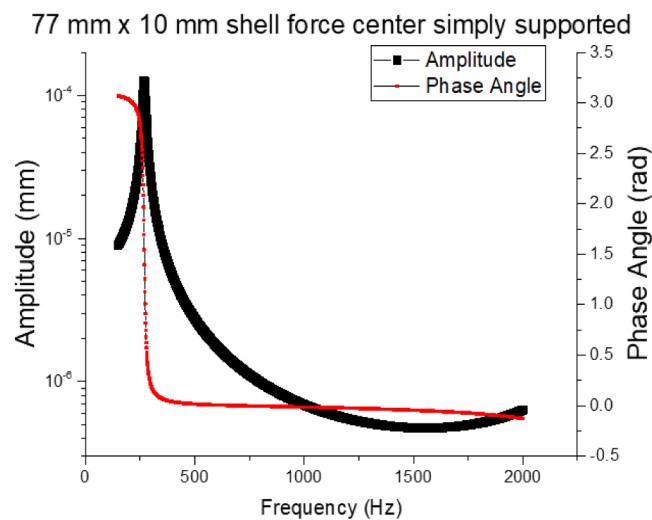

FIG. 8. X strain component in units of microstrain of a 70 × 10 × 0.67 mm^3 fixed-fixed BST beam using solid elements under a 4 Hz sinusoidal load showing one full cycle.

FIG. 7. Frequency domain response on a cut point (10,5) of a 77 × 10 × 0.67 mm pinned-pinned BST beam using shell elements with a resonant frequency at 268.94 Hz.
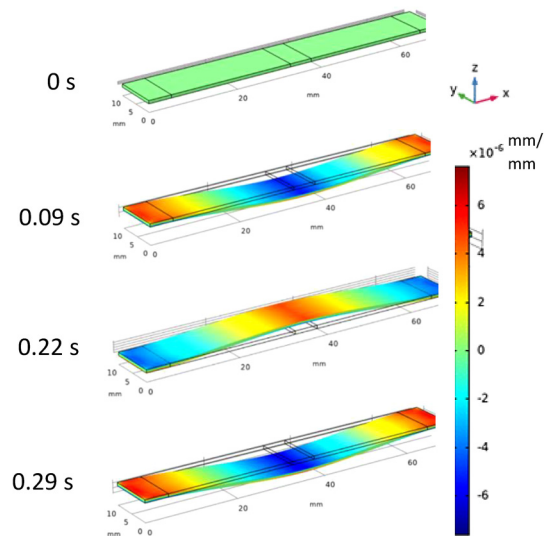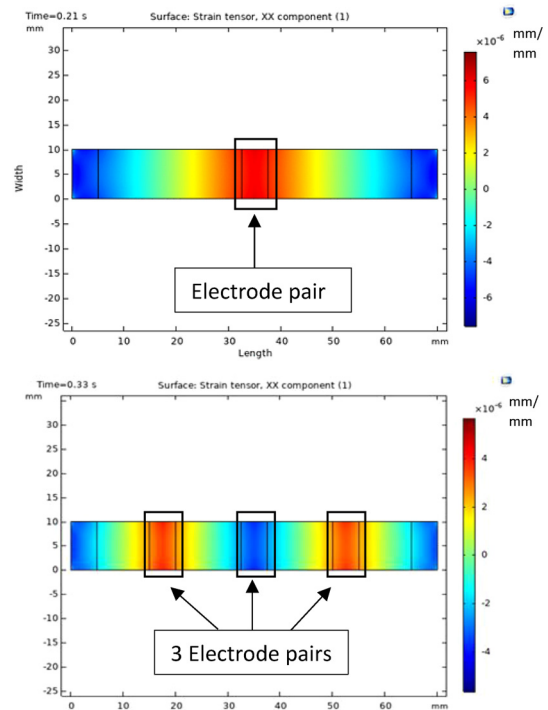

FIG. 9. Top: Top-down view of x-component strain in units of microstrain for a single bending point design near the peak strain of a cycle with a single central electrode pair. Bottom: Top-down view of x-component strain of a three bending point design near peak strain of a cycle with three pairs of electrodes.
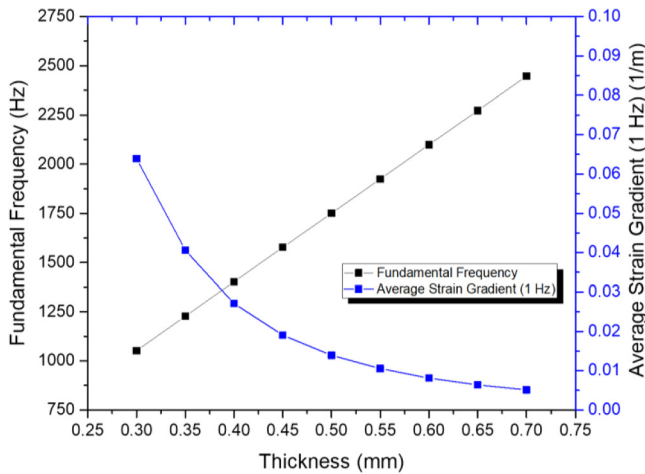
FIG. 10. The fundamental frequency and strain gradient of a $40 \times 10 \times X$ mm^3 beam as a function of thickness.

The fundamental frequency increases parabolically with an increasing number of bending points. The strain gradient decreases rapidly with increasing bending points. The blue data points represent a total electrode area (100 mm^2) distributed across all of the bending points, while the white data points represent a constant 50 mm^2 electrode area multiplied for each bending point. As the number of bending points increases, the fixed total electrode area produces a larger averaged strain gradient in most cases. That is, as electrode area increases, the strain gradient is reduced as a result of the reduction in strain gradient laterally from the bending point. However, the increase in collection area improves the overall charge output of higher bending point designs as demonstrated in Fig. 12.
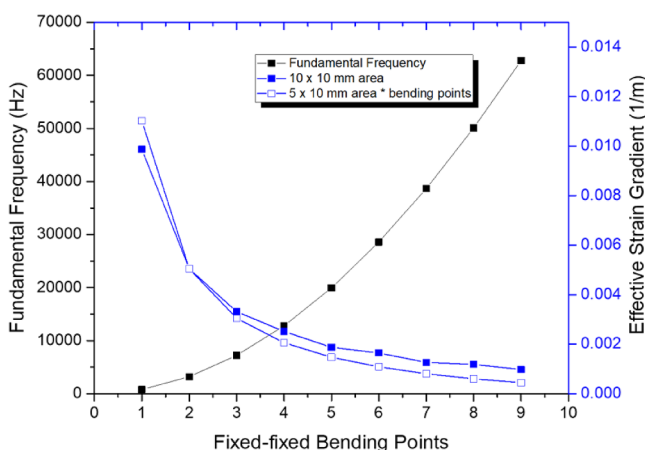

FIG. 11. The fundamental frequency and effective strain gradient for additional fixed-fixed bending points on a $70 \times 10 \times 0.70$ mm^3 beam.
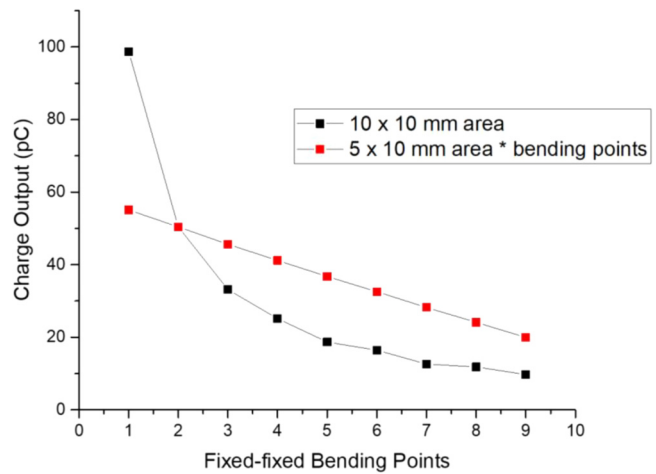

FIG. 12. The charge output (pC) of a normalized electrode area, 100 mm^2, as a function of the number of bending points and the charge output of an increasing electrode area of 50 mm^2 times the number of bending points. *No. of bending points assuming a flexoelectric coefficient of 100 μC/m.

The FEA results suggest that the flexoelectric output is maximized at low frequencies where the strain gradient is maximized. For higher frequency operation, devices need to harvest maximum charge by increasing electrode areas. The tradeoff between the flexoelectric output and the operational frequency will need to be optimized for the targeted operation.

V. CONCLUSION

BST ceramics with large flexoelectric coefficients, $\tilde{\mu}_{12}$, of $105.6 \pm 0.6\,\mu$C/m at room temperature were employed in a hydrophone with output sensitivities, $\sim$80 pC/N at the resonant frequency of 250 Hz. FEA was utilized to verify and predict resonant frequencies and in-plane strain gradients, allowing the design of optimal electrode placement and size. A three-bending point design outperformed a single bending point design by 43% based on charge output due to the increase in collection area. Voltage-based designs often produced inferior output compared to a charge-based design if connection in series is not utilized. FEA results also suggested maximum flexoelectric output at low frequencies. For higher frequency operation, larger electrode areas may be designed.

ACKNOWLEDGMENTS

DATA AVAILABILITY

The data that support the findings of this study are available from the corresponding author upon reasonable request.

REFERENCES

[1]B. Wang, Y. Gu, S. Zhang, and L. Q. Chen, "Flexoelectricity in solids progress, challenges, and perspectives," Prog. Mater. Sci. **106**, 100570 (2019).

[2]U. K. Bhaskar, N. Banerjee, A. Abdollahi, Z. Wang, D. G. Schlom, G. Rijnders, and G. Catalan, "A flexoelectric microelectromechanical system on silicon," Nat. Nanotechnol. **11**(3), 263 (2016).

[3]P. Zubko, G. Catalan, and A. K. Tagantsev, "Flexoelectric effect in solids," Annu. Rev. Mater. Res. **43**, 387 (2013).

[4]V. S. Mashkevich and K. B. Tolpygo, "Electrical, optical and elastic properties of diamond type crystals," Sov. Phys. JETP **5**, 435 (1957).

[5]S. M. Kogan, "Piezoelectric effect during inhomogeneous deformation and acoustic scattering of carriers in crystals," Sov. Phys. Solid State **5**(10), 2069 (1964).

[6]A. K. Tagantsev, "Theory of flexoelectric effect in crystals," Sov. Phys. JETP **61**, 1246 (1985).

[7]P. V. Yudin and A. K. Tagantsev, "Fundamentals of flexoelectricity in solids," Nanotechnology **24**(43), 432001 (2013).

[8]E. V. Bursian and O. I. Zaikovskii, "Changes in the curvature of a ferroelectric film due to polarization," Sov. Phys. Solid State **10**(5), 1121 (1968).

[9]L. Garten, "Residual ferroelectricity, piezoelectricity, and flexoelectricity in barium strontium titanate tunable dielectrics," Ph.D. dissertation (Department of Material Science and Engineering, Pennsylvania State University, 2014).

[10]B. Chu, W. Zhu, N. Li, and L. E. Cross, "Eric. flexure mode flexoelectric piezo-electric composites," J. Appl. Phys. **106**, 104109 (2009).

[11]W. Ma and L. E. Cross, "Flexoelectric polarization of barium strontium titanate in the paraelectric state," Appl. Phys. Lett. **81**, 3440 (2002).